Rainfall Distribution over Central and Southern Israel Induced by Large-Scale Moisture Flux

A. ISAKSON

Desert Meteorology Unit, Jacob Blaustein Institute for Desert Research, Ben-Gurion University of the Negev, Beer-Sheva, Israel

(Manuscript received 8 May 1995, in final form 1 February 1996)

ABSTRACT

A map of annual rainfall in Israel was obtained from the real-time calculation of the net condensation in large-scale moisture transport through the eastern Mediterranean, sea surface evaporation, and orographic condensation above the Judean mountain range. The averaged rainfall efficiency of condensation over the rainy season is assumed to be a function of the vertically and time-averaged temperature. The calculated rainfall map correlates well with statistical annual rainfall distribution, correlation coefficient 0.9, and allows the effect of the three sources of precipitation mentioned above to be estimated. The condensation within large-scale moisture transport, the main source of precipitation in the Israel region, yields approximately two-thirds of the bulk rainfall in the Mediterranean Sea shore region. The rest results from the contribution of the sea surface evaporation. Orographic condensation starts near the Mediterranean Sea shore and increases in the direction of the Judean mountains, where its contribution to rainfall is approximately equal to the contribution of the condensation within the large-scale moisture flux.

1. Introduction

The rainy period in Israel comes during the winter, and this annual rainfall (AR) is the only water source. In Fig. 1 the map of AR distribution averaged over a 30-year period is shown. Wolfson (1975) represented this distribution as a function of the latitude, the distance from the Mediterranean Sea shore, and terrain elevation, and he distinguished typical seashore zones, mountain zones, and southern desert zones. Zangvil and Druian (1990) proposed regioning based only on the southern decrease of AR and related it to the humidity decrease in large-scale flux through the Israel atmosphere.

Alpert and Shay-El (1993) and Shay-El and Alpert (1991) investigated the large-scale moisture flux through the eastern Mediterranean on the basis of the humidity and heat transfer equation and showed some paradox in distribution of the water vapor condensed in the atmosphere. Above the Israel Mediterranean Sea shore (the region of AR close to 600 mm), evaporation predominates during the rainy period, while above the Iraqi desert, condensation predominates. Alpert and Shay-El (1993) proposed cloud condensation and transport as an explanation of the phenomena. Thus, the rainfall efficiency (RE) of atmospheric condensation decreases quickly eastward from the Mediterranean Sea shore. The aforementioned rainy season average values of condensation represent only the difference between the mass of the condensed and evaporated water in the atmosphere, while the rainfall events should be correlated with time periods when condensation predominates. Then AR, in its turn, correlates with the bulk mass vapor condensed within such periods.

The orographic part of precipitation was studied by Alpert and Shafir (1989a,b, 1991) above an 20 km × 30 km area in the middle part of the Judean mountains. The orographic condensation (OC) was modeled as a result of the horizontal flux convergence in the planetary boundary layer inferred by additional vertical velocity of the interaction with terrain elevation (Alpert 1986). The orographic rainfall (OR) was estimated on the basis of the seasonal characteristic values of the ground surface temperature, lapse rate, humidity, and horizontal velocity. In calculations of AR distribution it is important to describe OR within the whole Judean mountain region by the modeling of OC in the moist air ascent process in real time, as performed for a mountain region in western Colorado (Rhea 1978) and for the Olympic Mountains (Barros and Lattenmaier 1993).

In this investigation, the rainfall distribution is described as a result of the condensation process within the large-scale moisture flux above Israel and the interaction of this flux with the Mediterranean Sea surface and the Judean mountain range. The mass condensed in the atmosphere was calculated by using the time- and space-integrated moisture budget equation. The time integration included only periods when condensation predominates. For the moisture transport de-

Corresponding author address: Dr. A. Isakson, Desert Meteorological Unit, Jacob Blaustein Institute for Desert Research, Ben-Gurion University of the Negev, Beer-Sheva, Israel.
E-mail: avigdor.bgumail.bgu.ac.il

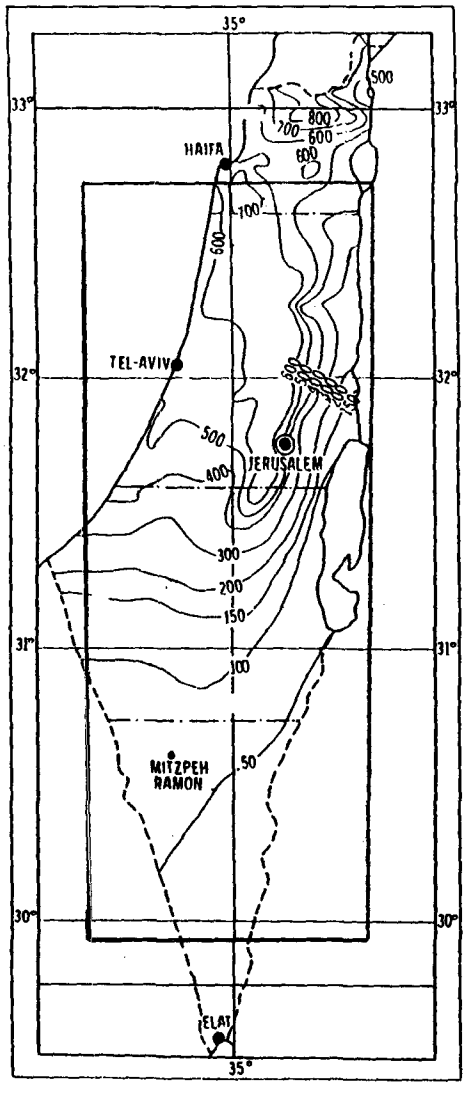

FIG. 1. Average annual rainfall (mm) in Israel (1951–80).

scription, the European Centre for Medium-Range Weather Forecasts (ECMWF) information, measured on 10 mandatory levels at 12-h intervals, was used. The Judean mountain region is small in comparison to the ECMWF grid step (see Fig. 2). The terrain elevation here is smaller than those in the mountain region in western Colorado and the Olympic Mountains mentioned above. In order to avoid the error involved in the modeling of vertical velocity, the prediction of OC in the present study was based on the tracing of the vertical displacement of an elementary volume as a function of its initial position. The rainfall distribution was obtained from the distribution of bulk condensation through the use of an RE coefficient, chosen as a linear function of latitudinal position varying between the respective values at Haifa and Eilat, which were extreme points of the region. Section 2 describes condensation in the moisture transport above the Israel region, section 3 contains calculation of the orographic rainfall in the Judean mountains region, section 4 describes the calculation of the map of AR distribution in Israel, and section 5 contains a discussion of the results and parameters of the model. A list of variables is given in the appendix.

2. Condensation in moisture transport through the Israel region

a. Equations

Evaluation of evaporation and condensation in the moisture flux is based on the moisture budget equation

$$\frac{\partial q}{\partial t} + \mathbf{v}\cdot\nabla q - \nabla\cdot(k\nabla q) = e - c = -h_q. \quad (1)$$

Here $\mathbf{v}$ is the wind velocity vector, q is specific humidity, k is the turbulent diffusivity coefficient, and e and c evaporation and condensation rates, respectively; their difference is the net condensation rate h_q.

Let Ω be a cylindrical domain extending vertically onto the pressure interval $p_1 < p < p_0$ above the surface of unit area S with boundary l. The mass of water vapor within Ω is

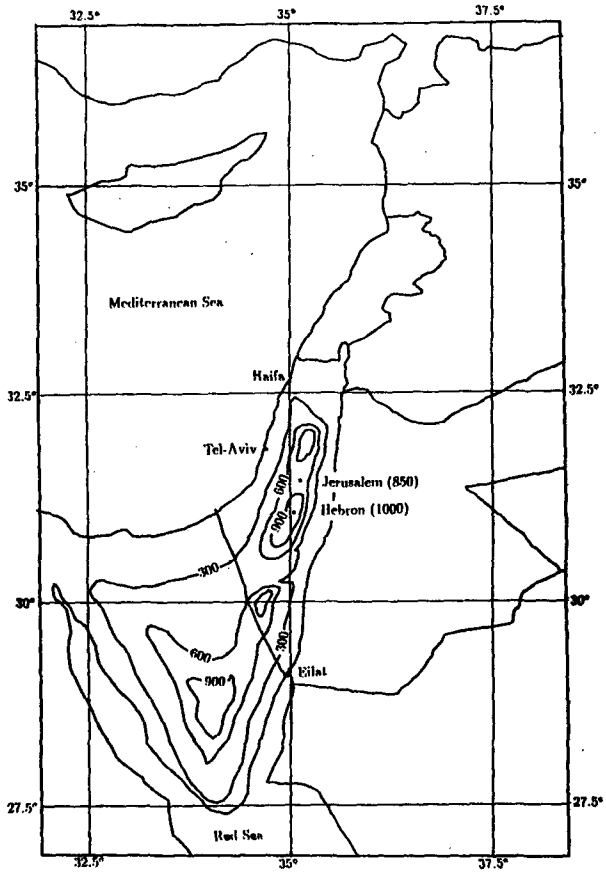

FIG. 2. Eastern Mediterranean with the ECMWF data grid.

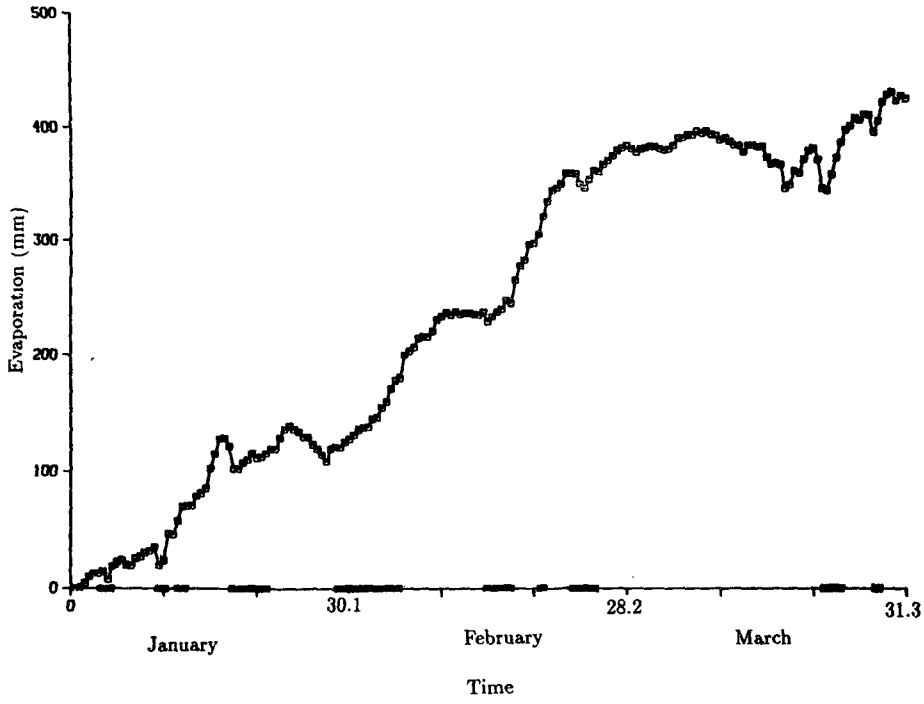

FIG. 3. The time dependence of the mass (mm) of water evaporated within the large-scale moisture flux above the 33.75°N, 33.75°E point. Periods of measured rainfall are shown on the time axis.

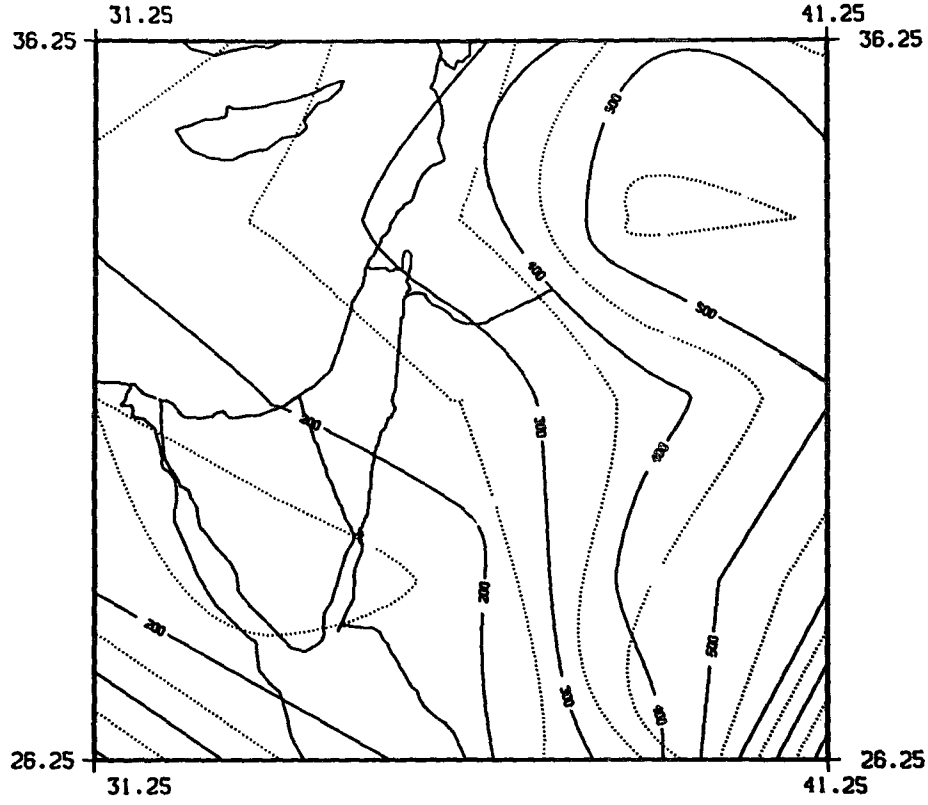

FIG. 4. Bulk condensation (mm) within moisture transport in the eastern Mediterranean in the period 1 January–31 March 1985.

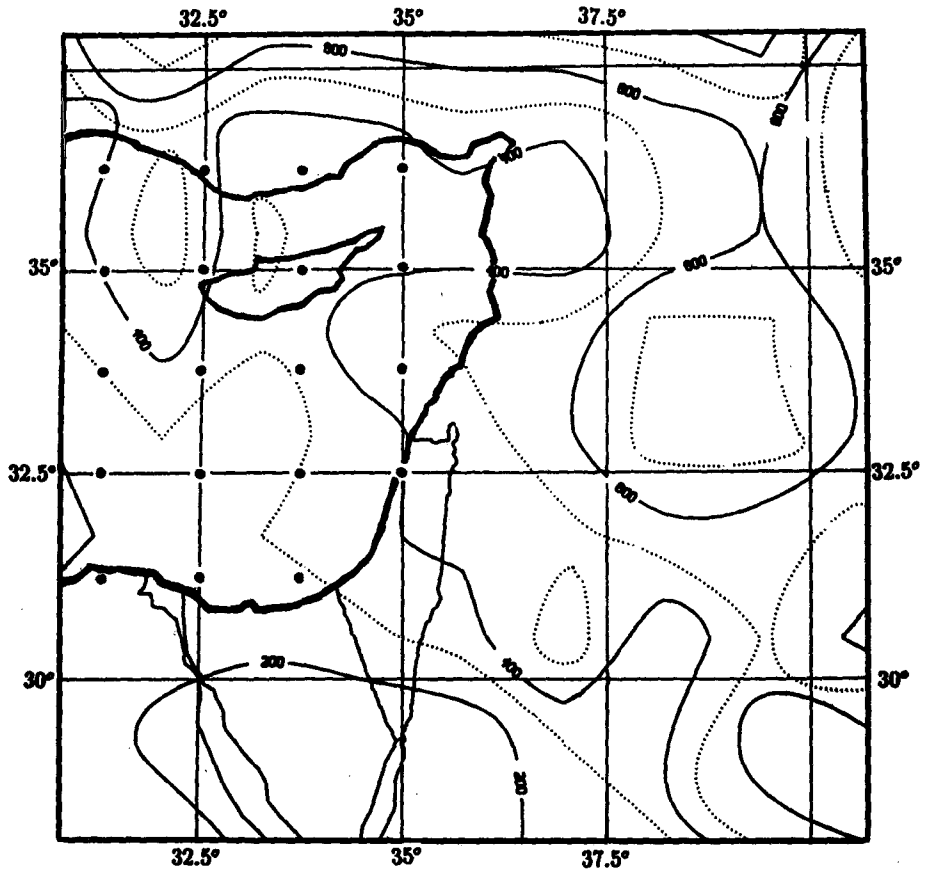

FIG. 5. Bulk condensation (mm) derived from moisture transport and sea surface evaporation in the eastern Mediterranean in the period 1 January–31 March 1985.

$$Q(t) = \frac{1}{g}\int_{\Omega} q dx dy dp.$$

The term by term integration of (1) divided by the gravity acceleration g yields for the volume Ω the following relation:

$$R(t) = \frac{1}{g}\int_{\Omega} h_q d\Omega = -\frac{\partial Q}{\partial t} - \frac{1}{g}\oint_l \int v_n q dp dl + E_s, \quad (2)$$

where $R(t)$ is the rate of variation of the water vapor mass within volume Ω, v_n is the normal to l component of the wind velocity, and E_s is some typical value of evaporation rate from a unit area of the bottom surface S. The terms of turbulent exchange through the vertical boundary and the upper horizontal surface are omitted in (2), as negligibly small compared to the transport ones.

In two cases to be treated below, the evaporation rate E_s may be easily estimated. The rate of evaporation from the sea surface into the moisture flux has been determined by the following expression (Liu et al. 1979):

$$E_s = \varrho C_e (q_s - q) U, \quad (3)$$

where ϱ is the air density, U and q are the air velocity and specific humidity at the height of 2 m, q_s is the specific humidity of saturation at sea surface temperature, and $C_e = 1.4 \times 10^{-3}$ is a dimensionless coefficient. The evaporation rate from a desert surface will be supposed to be negligible compared to that from the sea surface.

Integration of Eq. (2) within time period $[t_1, t_2]$ yields the following equation for the calculation of the bulk mass of condensed vapor (or evaporated water) within volume Ω:

$$\int_{t_1}^{t_2} R(t) dt = \frac{1}{g}\int_{t_1}^{t_2}\int_{\Omega} h_q d\Omega dt = -\frac{1}{g}\int_{t_1}^{t_2}\oint_l \int v_n q dl dp dt + \int_{t_1}^{t_2} E_s dt, \quad (4)$$

where the value

$$\int_{t_1}^{t_2} \frac{\partial Q}{\partial t} dt = Q(t_2) - Q(t_1)$$

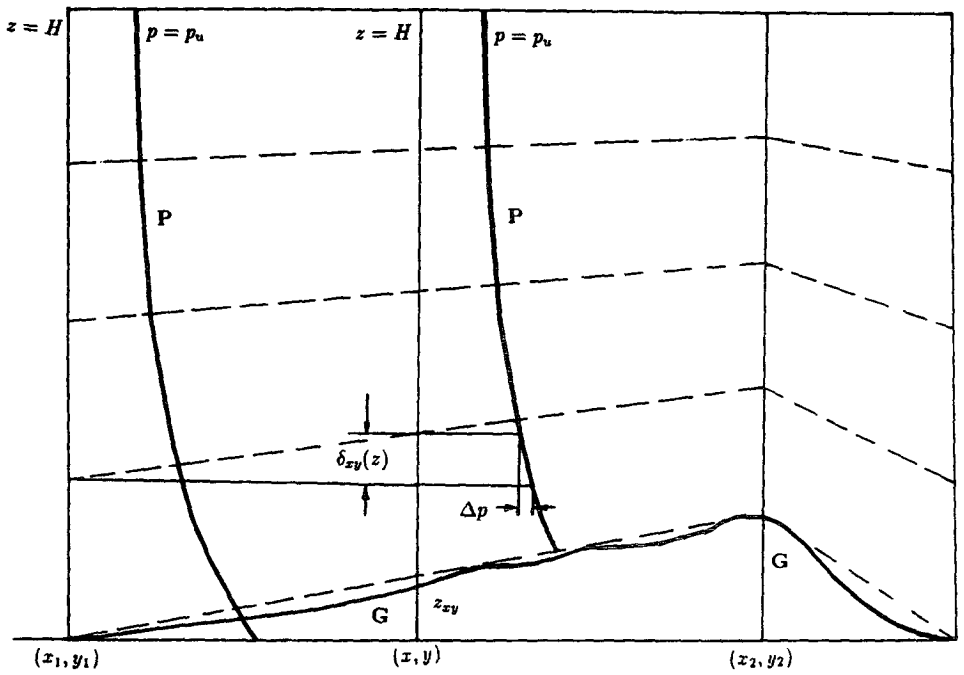

FIG. 6. Pressure distribution (P) and streamlines (dashed lines) in the moisture flux interaction with terrain elevation (G).

has been omitted as negligible relative to flux integration terms. This equality expresses the obvious fact that if the humidity storage process is negligible, the total mass of condensed vapor is the difference between inflow and outflow vapor mass. The ground surface evaporation is part of the inflow vapor mass.

b. *Calculation procedure and condensed vapor distributions*

The moisture flux over Israel is represented by ECMWF/World Climate Research Programme level III-A data, containing the 0000 and 1200 UTC gridded (2.5°, 2.5°) upper-air temperature, relative humidity, geopotential and wind field near the surface and at 10 mandatory pressure levels up to 100 mb.

The integral term of the rhs of (4) was calculated at the definite time of the ECMWF measurements within every grid cell by use of the vertical distributions of humidity and horizontal velocity in four grid points, and the result was divided by the cell surface area. The positive sense of integration has been chosen so that the positive value of the integral corresponds to predominant evaporation and the negative value to predominant condensation in accordance with (4).

The numerical procedure of the time integration used in (4) is the summing of function values at every time moment of the ECMWF measurement within period $[t_1, t_2]$ and multiplying by 12 h, the time interval of the measurements.

When $t_1 = 0$ and $t_2 = t$, the integral on the rhs of (4) is the function of t, which represents the mass of evaporated (or condensated) vapor as a function of time. The time series shown in Fig. 3 is the function calculated in this way for the volume above the grid cell with the center in the point (33.75°N, 33.75°E), the atmospheric cell above the sea surface nearest to Israel.

It is obvious that the evaporation process predominates. The same fact was described by Shay-El and Alpert (1991) in terms of the values of net condensation averaged over the rainy period. The total mass of the evaporated water within a three-month period is approximately 450 mm, while the sea surface evaporation within the same period, calculated at grid point (32.5°N, 32.5°E) by use of (3) and ECMWF surface data, is approximately 300 mm, in accordance with statistically averaged measured values (Rosenan and Gilead 1985). Alpert and Shay-El (1993) found that above the Arabia–Iraqi desert the condensation process predominates, and they explained this phenomenon by the cloud formation and transport. The above-mentioned difference between the evaporation in the atmosphere and the sea surface evaporation should be likely related to the cloud evaporation.

The first term on the rhs of (4) presents the condensation (or evaporation) that takes place within the large-scale moisture flux, and the second term is the part of the condensed vapor mass, caused by the sea surface evaporation. The intervals of decrease on the graph in Fig. 3 are the time periods in which the condensation process predominates and the net condensation in the large-scale moisture flux is positive. The rain

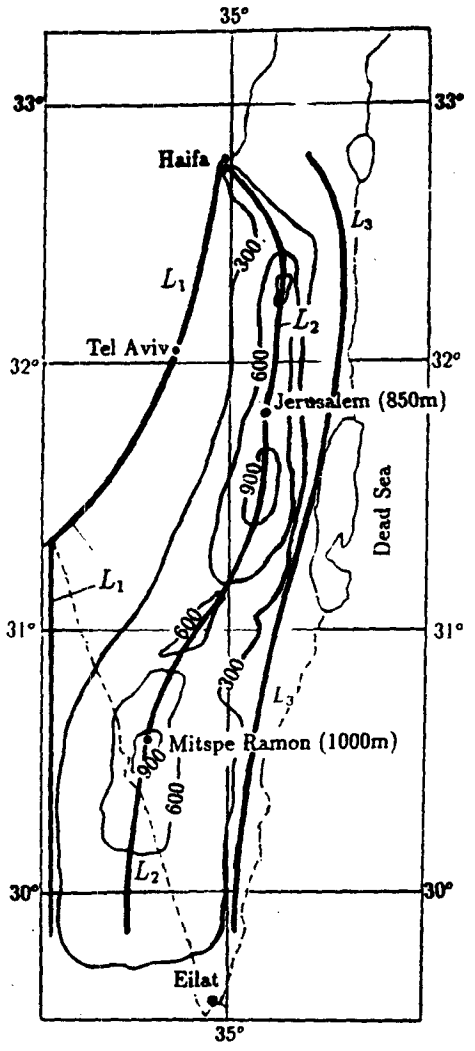

FIG. 7. Topography of the Judean mountain region with lines of the ascent beginning L_1, the maximal terrain elevation L_2, and the end of moisture flux interaction L_3.

events caused by the large-scale moisture transport are connected with such time periods (see Fig. 3), which are specific for every grid-cell volume. Note that the condensation events in the time series in Fig. 3 are related to the atmosphere above the area of one ECMWF grid cell. The latter is much larger than Israel's seashore between Tel Aviv and Haifa to which the measured rainfall relates. Thus, the correspondence is expected to be qualitative, which it is. If the time integration of the integral term on the rhs of (4) includes only time intervals when the space integral is negative, the result is the bulk mass of the net condensed vapor in condensation events. This operation was performed for every grid cell volume in the region, and the result was related to the cell center. The distribution of the net condensation mass within the large-scale moisture flux, shown in Fig. 4, was obtained in this way.

The north gradient of the condensed vapor mass is clear. This phenomenon may be connected with the south gradient of vertically averaged temperature shown further in section 4. The eastern gradient of the condensed vapor mass may be easily seen too.

The evaporation term in the rhs of Eq. (4) is always positive in volumes above the sea surface. The addition of this value enlarges the mass of condensed vapor during every condensation event and makes the duration of the condensation process longer. The Israel territory includes two ECMWF grid points. The distance from the point (32.5°N, 35°E) to the seashore (10 km) is ≈3% of grid step. For simplification of interpolation operations, this point was regarded as that of the sea surface, with the sea surface temperature as in point (32.5°N, 32.5°E), the sea surface grid point nearest to the Israel shore. The second grid point within Israel is inland of the seashore by about 170 km and is located in a desert region. For this point the surface evaporation was neglected. The Mediterranean Sea boundaries were defined as shown in Fig. 5, and for the sake of precision, the calculation was performed on a grid of 1.25° × 1.25°, for which the seashore is clear to the grid lines. The integration on the rhs of (4) has been performed in all time intervals when the rhs of (4) is positive. This procedure has been carried out for every grid cell in the region. This calculation yields the distribution shown in Fig. 5. The comparison of the distributions at the point (32.5°N, 35°E) shows that, during the three months under consideration, the sea evaporation accounts for approximately one-third of the bulk condensation near the seashore in Israel.

3. Orographic rainfall

a. Model

The model of the moisture flux interaction with the relief describes the process of adiabatic ascent within the lower layer of atmosphere. Values of meteorological parameters were assumed constant within 12 h between two ECMWF measurements. Vertical distributions of temperature, humidity, and components of horizontal velocity were interpolated from gridded ECMWF data. The Israel Meteorological Service performs soundings for the ECMWF dataset near Tel Aviv. Thus, these parameters were interpolated within approximately one grid step near the point of direct measurement. The airflow instability induced by mountain valleys or by heating and cooling of slopes is neglected because the horizontal scale of this instability is much shorter than the length of the Judean mountains range and the horizontal scale of the ECMWF data. The influence of the moisture flux interaction with terrain spreads up to the height H or up to the pressure p_u, which are the parameters of the model (Fig. 6).

The flux ascent begins at point (x_1, y_1, z_1), where x_1 and y_1 horizontal coordinates and z_1 is the terrain elevation. The ascent direction is determined by the vertically averaged wind velocity

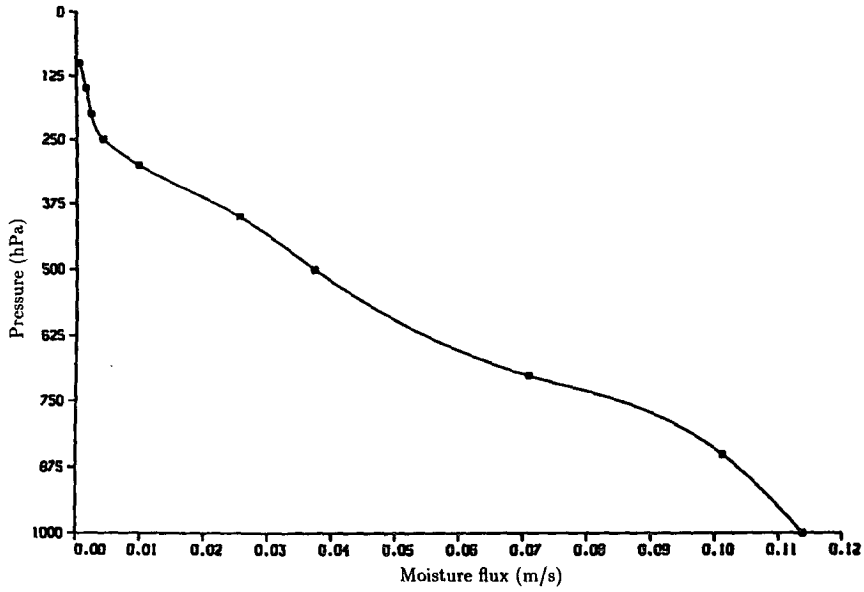

FIG. 8. The vertical distribution of the total moisture flux from the Mediterranean Sea on 22 February 1985.

$$\mathbf{v}_m = \frac{1}{p_s - p_u} \int_{p_u}^{p_s} [U(p), V(p)]\, dp. \qquad (5)$$

The large-scale moisture flux direction, thus determined, varies slowly within the Judean mountain region for a fixed time moment. The distance of the moist air ascent is no more than 50 km, so the effect of the crossing of ascent trajectories beginning at different points is negligible. Ascent process continues up to the point (x_2, y_2, z_2) of the maximal terrain altitude in the $\mathbf{v}_m$ direction. The altitude z_{xy} at the intermediate point (x, y) is defined by linear interpolation:

$$z_{xy} = \frac{r_{xy}}{r_{12}} z_2 + \left(1 - \frac{r_{xy}}{r_{12}}\right) z_1, \qquad (6)$$

where r_{12} is the distance between the points (x_1, y_1) and (x_2, y_2), and r_{xy} is the distance from (x, y) to (x_1, y_1).

When an elementary volume of moist air ascends near the ground surface, the variation of the vertical coordinate is maximal and is $z_{xy} - z_1$, while at $z = H$ it is zero. The upper limit of the moisture flux interaction with terrain, H, is much higher than terrain elevation $H \gg z_{xy}$ (Fig. 6). The change $\delta(z)$ of the initial height z in the ascent process has been assumed to be the linear func-

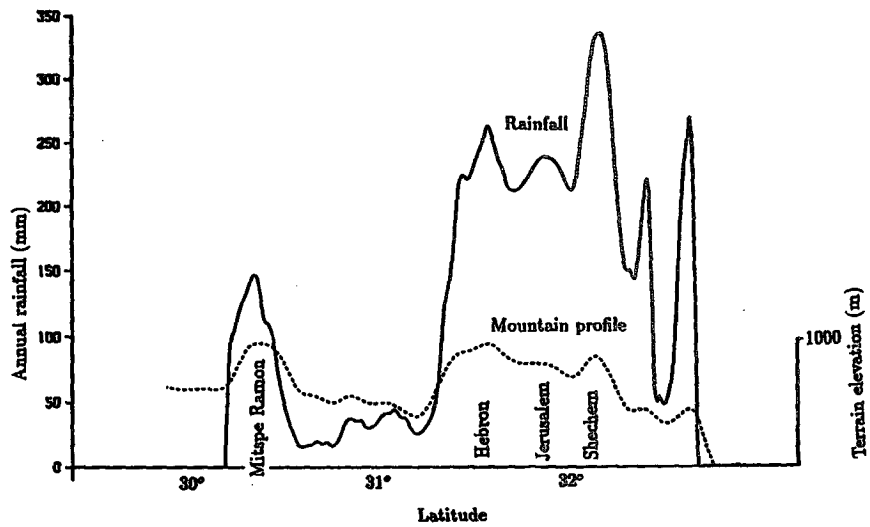

FIG. 9. Calculated distribution of the orographic rainfall (mm) along the Judean mountain summits in the period 1 January–31 March 1985.

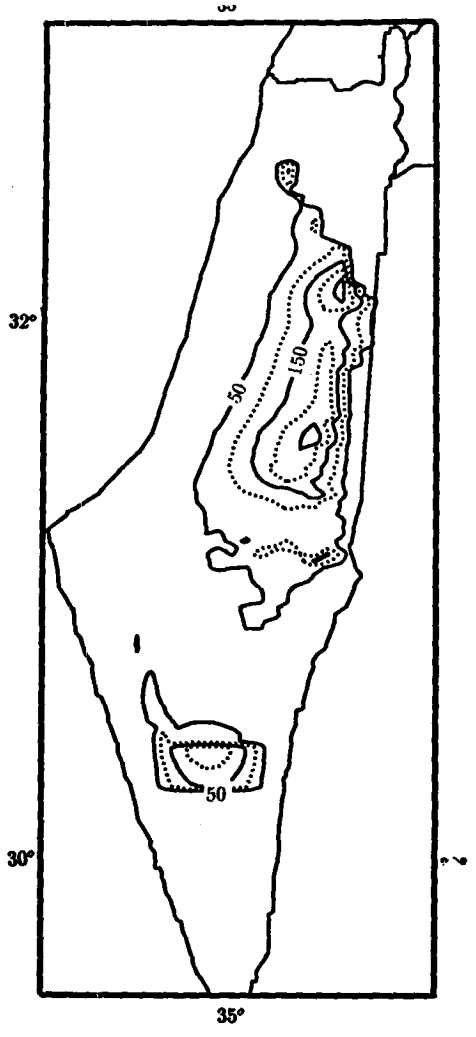

FIG. 10. The calculated orographic rainfall (mm) in the Judean mountains region in the period 1 January–31 March 1985.

tion of z, decreasing from the maximal value on the ground surface up to zero at height $z = H$:

$$\delta_{xy}(z) = (H - z)\frac{z_{xy} - z_1}{H - z_{xy}}.$$

The vertical coordinate z and pressure p are connected by the equation

$$p = p_0 \exp\left(-\frac{z}{G_p}\right), \quad G_p = 7995.7 \text{ m}.$$

The value of G_p is in regard to a ground surface temperature at 0°C, but a simple estimation of the relative errors shows that the difference in G_p values for the rainy season is negligible. The mean sea level pressure p_0 may be calculated from geopotential vertical distribution given at ECMWF data mandatory levels:

$$p_0 = 1000 + \frac{150}{G(850) - G(1000)} G(1000),$$

where $G(p)$ is the geopotential vertical distribution in the pressure coordinate.

The pressure p in elementary volume at height z above point (x_1, y_1) changes above point (x, y) to

$$p + \Delta p = p_0 \exp\left\{-\frac{[z + \delta(z)]}{G_p}\right\}.$$

Then, the ratio $d_{xy}(z)$ of the pressure to its initial value within the elementary volume above point (x, y) is

$$d_{xy}(z) = \frac{p + \Delta p}{p} = \exp\left[-\frac{\delta(z)}{G_p}\right],$$

or, using the pressure coordinate,

$$d_{xy}(p) = \left(\frac{p_u}{p}\right)^{(z_{xy}-z_1)/(H-z_{xy})}. \tag{7}$$

Most of the line from which the ascent begins is along the Mediterranean Sea shore, where $z_1 = 0$, and the latter relation may be written more simply as

$$d_{xy}(p) = \left(\frac{p_u}{p}\right)^{z_{xy}/(H-z_{xy})}.$$

The change of the temperature in the ascending volume is modeled below by the equation of dry-adiabatic ascent for simplicity only. The effect of humidity may be easily taken into consideration. The temperature $T_1(p)$ at the beginning of the ascent changes to

$$T_{xy}(p) = [d_{xy}(p)]^{0.286} T_1(p) \tag{8}$$

in elementary volume above point (x, y). The part of the specific humidity condensed during adiabatic ascent up to point (x, y) may be found from following the system of equations (Haltiner and Wiliams 1980)

$$LC_{xy}(p) = c_p \delta T,$$

and

$$q_{xy}(p) - C_{xy}(p) = q_s(T + \delta T, p),$$

coupled with the conservation condition for $q_1(p)$—specific humidity distribution above the point (x_1, y_1)—

$$q_{xy}(p) + C_{xy}(p) = q_1(p),$$

where L is the latent heat of vaporization, c_p is the specific heat of constant pressure, and q_s is the specific humidity of saturation. Elimination of q_{xy}—the specific humidity distribution above point (x, y)—yields the following system of equations for $C_{xy}(p, t)$:

$$LC_{xy}(p) = c_p \delta T,$$

and

$$C_{xy}(p) = \frac{1}{2}[q_1(p) - q_s(T + \delta T, p)]. \tag{9}$$

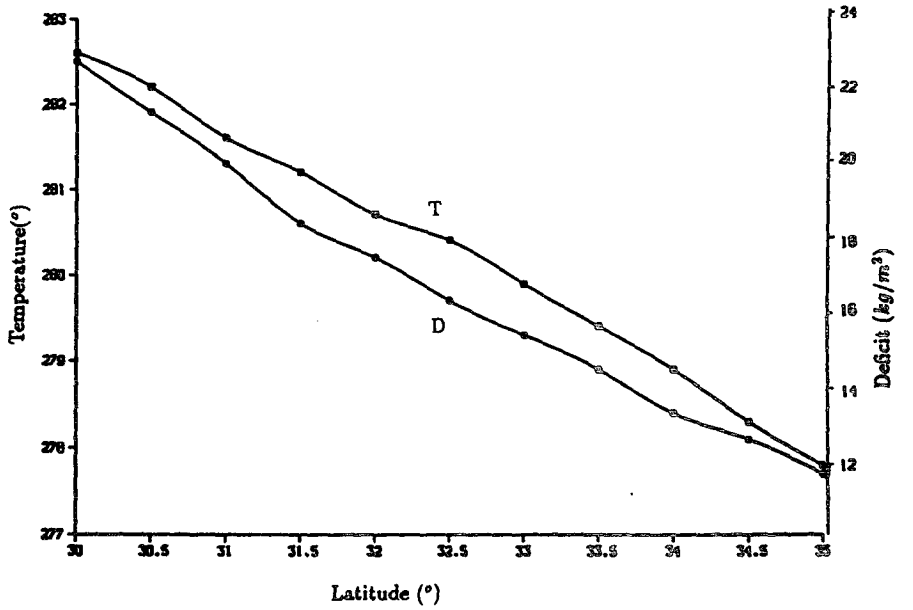

FIG. 11. The latitudinal distribution of the vertically (1000–700 hPa) and time- (1 January–31 March 1985) averaged temperature (T) and time-averaged moisture deficit in the 1000–100-hPa layer (D).

One can see that variations of p and T during the ascent process depend on horizontal distance from the point of the ascent beginning, and thus they are functions of time. The total mass of the condensed vapor within the ascending layer above the point (x, y) is

$$S_{xy}(t) = \frac{1}{g}\int_{p_u}^{p_x} R_{xy}(p, t)dp,$$

where function R_{xy} is the positive part of $C_{xy}(p, t)$:

$$R_{xy} = \begin{cases} C_{xy}, & C_{xy} > 0 \\ 0, & C_{xy} < 0. \end{cases}$$

The condensation rate F_{xy} within the ascending moisture layer above point (x, y) may be calculated as the material time derivative of S_{xy}:

$$F_{xy} = \frac{dS_{xy}(t)}{dt} = \frac{1}{g}\int_{p_u}^{p_x} \frac{dC_{xy}(p, t)}{dt}\,dp$$

$$= \frac{1}{g}\int_{p_u}^{p_x} \mathbf{v}\cdot\nabla C_{xy}(p, t)dp$$

$$\approx \frac{1}{g}\mathbf{v}_m\cdot\nabla\int_{p_u}^{p_x} C_{xy}(p, t)dp \approx \mathbf{v}_m\cdot\nabla S_{xy}, \quad (10)$$

where $\mathbf{v}_m$ is the vertically averaged wind velocity vector defined by (5).

System (9) includes the large parameter L/c_p, the latent heat of vaporization related to the specific heat of constant pressure. The function $q_s(t, p)$ is nonlinear. The error of the first term on the rhs of this equation, $q_1(p)$, which is the vertical distribution of specific humidity, is determined by ECMWF data and interpolation procedure errors. In the course of numerical solution of system (9), p is fixed and this term is constant. The accuracy of the solution is thus determined by the nonlinear term. It is better to solve numerically one nonlinear equation received after elimination of C_{xy} to avoid the large parameter in nonlinear function argument. The solution accuracy was chosen so that function S_{xy} was calculated with at least 5% accuracy.

b. Calculation procedure and resulting distributions

The Judean mountains form an approximately meridionally oriented range, 200 km long and 50 km wide, with maximal elevation approximately 1000 m in the middle and southern parts. The width-to-length ratio is approximately 0.25, and the height-to-width ratio is 0.02 (Fig. 2).

Components of the horizontal moisture flux in 1000–700-mb layer at the point (35°, 32.5°), time averaged over the period 1 January–31 March 1985, are

$$\frac{1}{t}\int_0^t \left\{\frac{1}{g}\int_{700}^{1000} q(p)[u(p), v(p)]dp\right\}dt$$

$$= (272, 63) \quad \text{kg m}^{-1}\,\text{s}^{-1}, \quad (11)$$

where (u, v) is the horizontal velocity vector and q is specific humidity. The time-averaged direction of the flux is very close to the west–east one. All relatively strong winds during the rainy period are in the interval 230°–310°. The rainfall events connected with south-

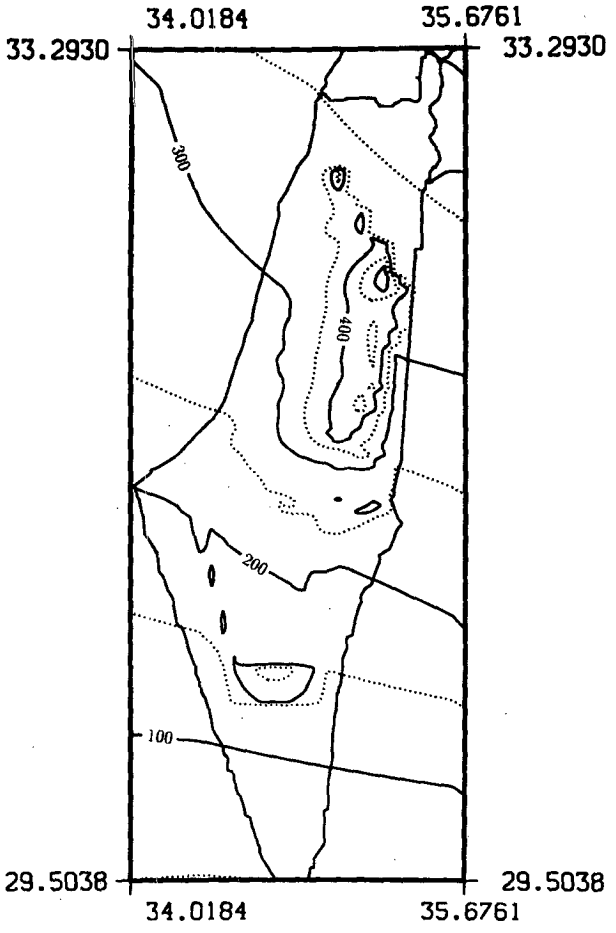

FIG. 12. Calculated rainfall (mm) in Israel in the period 1 January–31 March 1985.

eastern humidity transport, such as the rainstorm on 22 March 1985, are included within this angle interval, although the model deals with the interval 190°–350°.

Thus, the zone of OC is placed between Israel's western border, line L_1, and the Judean mountain range, line L_2 (see Fig. 7). It is convenient to represent every curve in the form $[x(y), y, z(y)]$, using local Cartesian coordinates x (longitude), y (latitude), and z (terrain elevation). Functions $x(y)$ and $z(y)$ were determined by the values in the 10-km interval for the y coordinate and afterward interpolated by a cubic spline. Between lines L_1 and L_2, L_2 and L_3 terrain elevation was linearly interpolated.

A typical vertical distribution of humidity flux is presented in Fig. 8. The bulk of the water vapor transport occurs in the layer between the surface and approximately the 650-mb level. Thus, it is natural to choose $p_u = 500$ mb, in order to include the layer of maximum moisture transport.

The calculation procedure, described in the previous section, has been performed on the grid within the Judean mountain region. Points of ascent beginning are always on line L_1, and points of maximal elevation are disposed on line L_2. For every grid point between these two lines, the initial and end points are determined by wind direction in (5).

The choice of the grid step mostly depends on the function S_{xy} differentiation in (10). If the moisture flux is near saturation before the beginning of the ascent, the function S_{xy} may be fast increasing in the ascent direction. It is monotonic in this direction, but may be rather complicated because of the topography. The grid step was decreased to the value yielding the 5% accuracy to the main distributions described below.

Numerical calculations were performed on a 50×130 grid in the Judean mountain region (see Fig. 7). For every grid point, the nonlinear system (9) was solved at 10 pressure levels, and a condensation rate has been defined from (10) by numerical differentiation. This value of the condensation rate was assumed to last during the 12-h time interval of the ECMWF data and was integrated within all intervals when it was positive.

The rate of OR, P_{xy}, at a surface point (x, y) is defined as proportional to the condensation rate above this point (Rhea 1978; Alpert 1986):

$$P_{xy} = KF_{xy}.$$

The coefficient of orographic rainfall efficiency K then connects the bulk values of OC and OR. Only the travel time of ascending moist air was taken into consideration in the definition of K.

The ascent time of an elementary air volume above the Judean mountains, if the horizontal velocity is of 10 m s^{-1}, is no more than 1 h. Then the time, or the distance, from the beginning of the ascent is a valid parameter in the orographic part of every rainfall event. The estimation of K is simpler for the annual OR. The averaged moisture flux is clearly easterly in direction [see Eq. (11)], and for the surface point with local coordinates (x, y), the averaged ascent time is proportional to the distance from the line L_1 in the x (longitude) direction. Therefore, the value of K may be calculated as

$$K = A\frac{x - x_1}{x_0 - x_1}, \qquad (12)$$

where x_1 is the local x coordinate of the point on the line L_1 with the same local latitude y. The value x_0 is the local longitude of Jerusalem, which is the eastern point of the line L_2. Thus, the value of K is 0 on line L_1 and is maximal on L_2. The choice of A, which is the maximal portion of the condensed vapor that yields precipitation, is based on statistical model of Wolfson (1975). This model estimates the growth of annual rainfall with terrain elevation in the middle and northern regions of Israel as being 26 mm per 100-m elevation. Thus, the annual orographic rainfall at Jerusalem (850 m) is approximately 250 mm, and the value of A ought to be chosen as 0.4. Because the rainy period in the Judean mountain region includes December and even part of November in addition to the three months under consideration, it may be accepted that no more than 30% of the water condensed during adi-

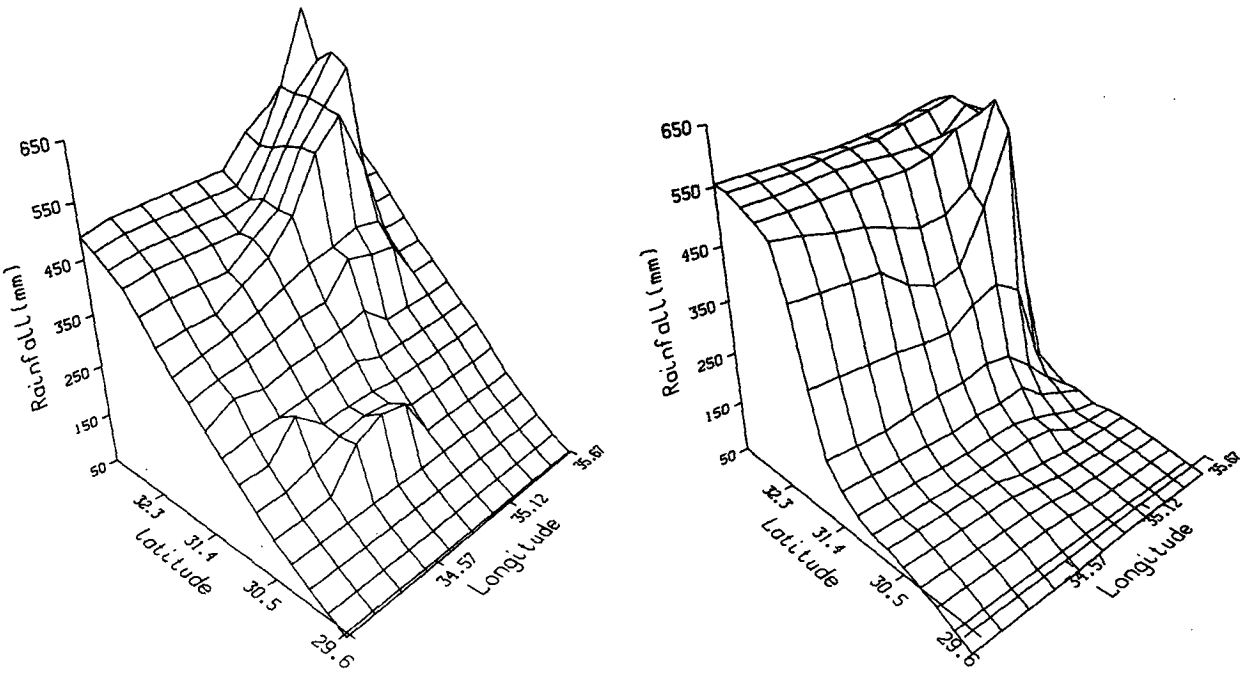

FIG. 13. (a) Calculated annual rainfall over Israel. (b) Average measured annual rainfall distribution (Fig. 1) above the marked rectangle.

abatic ascent above the Judean mountains yields orographic rainfall.

The distribution of the annual OR at the points of maximum elevation along the Judean mountains, calculated with the thus-determined coefficient K, is shown in Fig. 9. The absolute elevation of the southern end of the mountain range is equal to the elevation at the middle but receives less orographic precipitation. One of the reasons is smaller relative elevation and travel time. The second reason is the southern gradients of temperature and moisture deficit, which will be described and discussed in section 4. The map of the orographic rainfalls, calculated with K and defined by Eq. (12), is shown in Fig. 10.

4. Rainfall distribution

The distribution of rainfall in the three-month period under consideration was derived from the calculated distribution of water vapor condensation with an RE coefficient, similar to the one defined above for orographic rainfall. The time-averaged RE was assumed to depend only on the vertically spaced and time-averaged temperature. The humidity deficit in the moisture flux—that is, the mass of water vapor deficit to the saturation state—has been calculated as follows:

$$D = \frac{1}{g}\int_{100}^{1000} (q_s - q)\,dp, \qquad (13)$$

where q_s is the specific humidity of saturation. Alpert and Shafir (1989a) noted the great south temperature gradient during the rainfall events they investigated. In Fig. 11, the time-averaged value of deficit is presented together with the time- and height- (700–1000 hPa) averaged temperature as functions of latitude. The decrease of the deficit with latitude indicates that the RE of the condensation process within the large-scale moisture flux must be much greater in the northern part of the region. The latitude distributions of the vertically and time-averaged temperature and water vapor deficit show that the latter increases with an increase in temperature, and both are nearly linear functions of the latitude in the Israel region. Thus, RE as a function of temperature was chosen as a linear function of latitude, defined by the two extreme points, Haifa and Eilat.

The considered period from January to March 1985 includes more than 30 measured rainfall events in Israel and covers the entire rainy season in the southern part of the region. The measured rainfall during this period was 149.7 mm at Haifa and 11.3 mm at Eilat (Israel Meteorologic Service 1985). Thus, the two values of the RE function are approximately 0.36 and 0.12, respectively. The sum of the condensation presented in Fig. 5 and the orographic rainfall presented in Fig. 10 have been multiplied by the value of RE at every point. This yields the calculated distribution of rainfall within the three-month period under consideration, as shown in Fig. 12.

For the sake of comparison with the 30-yr-averaged annual rainfall distribution (Fig. 1), the calculated and the measured values of rainfall were reduced to the entire rainy period by means of a factor representing the ratio of rainfall, measured during the three months under consideration, to its averaged value. This factor, too, was chosen to be a linear function of the latitude

with values of $600/149.7 \approx 4$ and $15/11.3 \approx 1.4$ at Haifa and Eilat, respectively. [The statistically averaged AR is 600 mm at Haifa and 15 mm at Eilat (Rosenan and Gilead 1985).] The AR distribution thus calculated is presented in Fig. 13a. Measured AR distribution, shown in Fig. 1, was mapped on a grid of 15 $\times$ 21 points. Its main part, within the rectangle shown in Fig. 1, is presented in Fig. 13b. Comparison was performed at $11 \times 17 = 187$ inner points of the rectangle. The resulting correlation coefficient for the rainfall distribution shown in Fig. 12 and the 30-yr-averaged distribution in Fig. 1 were found to be 0.9. The reduction of the calculated distribution to the entire rainy period described before is a linear transform of the three-month-period distribution and cannot change the correlation coefficient. Its value for distribution shown in Figs. 13a and 13b remains 0.9.

The distributions, presented in Figs. 4, 5, and 12 allow estimation of the contribution of each process to rainfall formation at every point of the territory. For example, in the region of the Judean mountains summit the orographic rainfall yields approximately one-half of the total value.

5. Conclusions

This model represents AR distribution in the Israel region as the sum of three sources: the condensation process within the large-scale moisture flux, the sea surface evaporation, and the interaction of the large-scale moisture flux with the terrain. The latter depends on vertical and horizontal temperature distributions. The influence of the sea surface temperature on precipitation in Israel, described statistically by Tzvetkov and Assaf (1982) and found in Brenner's (1993) numerical experiments, easily follows from (3). Note that additional rainfall depends on other parameters of this equation.

The variation of the sea surface temperature, for example, may be compensated by the air temperature near the sea surface, or the additional rainfall may be the consequence of the lower air temperature, while the sea surface temperature is the same. The interaction of the large-scale moisture flux with the Mediterranean Sea surface based on ECMWF data and a correlation with rainfall measurement may be the subject of a special investigation.

The condensed vapor distribution shown in Fig. 5 reflects the role of the condensation process within large-scale moisture flux, which depends particularly on the temperature through other parameters. However, the difference between the rainfall in the southern and northern parts of Israel is related to the southern temperature gradient in the large-scale moisture flux, resulting in an RE gradient. The eastern decrease of the latter is not available within the Israel territory because of the Judean mountains.

In moisture budget calculations, no information on cloud water transport was used. Taking into account this factor may change the estimate on RE. However, since the temperature is a control parameter in the cloud formation process too, linear dependence of RE on the latitude may be a suitable approximation.

APPENDIX

List of Variables

AR	annual rainfall
$C_{xy}(p)$	condensed part of humidity
c	condensation rate
c_p	specific heat of constant pressure
D	humidity deficit in moisture flux—that is, the mass of water vapor deficit to the saturation state
d_{xy}	the ratio of the pressure within ascending elementary volume to its initial value above point (x, y)
$\delta(z)$	change of the initial height z in the ascent process
E_s	typical value of evaporation rate from a unit area
e	evaporation rate
F_{xy}	rate of OC above a surface point (x, y)
H	maximal height where the moisture flux interaction spreads with terrain
h_q	net condensation rate
K	orographic condensation rainfall efficiency
k	turbulent diffusivity coefficient
L	latent heat of vaporization
OC	orographic condensation
OR	orographic rainfall
P_{xy}	rate of OR at a surface point (x, y)
p_u	pressure at the maximal height of the moisture flux interaction with terrain
Q	mass of water vapor within volume Ω
q	specific humidity
q_s	specific humidity of saturation
RE	rainfall efficiency
$R(t)$	rate of variation of the water vapor mass within volume Ω
R_{xy}	positive part of $C_{xy}(p)$
$S_{xy}(t)$	total mass of the condensed vapor within the ascending layer above the point (x, y)
T	temperature
$\mathbf{v}$	velocity vector
x	local longitude
y	local latitude

REFERENCES

Alpert, P., 1986: Mesoscale indexing of the distribution of orographic precipitation over high mountains. *J. Climate Appl. Meteor.*, **25,** 532–545.

——, and H. Shafir, 1989a: Meso-γ scale distribution of orographic precipitation: Numerical study and comparison with precipitation derived from radar measurements. *J. Appl. Meteor.*, **28,** 1105–1117.

——, and ——, 1989b: A physical model to complement rainfall normals over complex terrain. *J. Hydrol.*, **110,** 51–62.

——, and ——, 1991: Role of detailed wind–topography interaction in orographic rainfall. *Quart. J. Roy. Meteor. Soc.*, **117B,** 421–427.

——, and Y. Shay-El, 1993: The paradox of the winter net moisture sink over the Arabian–Iraqi desert. *Ann. Geophys.*, **11,** 190–194.

Barros, A. P., and D. P. Lettenmaier, 1993: Dynamic modeling of the spatial distribution of precipitation in remote mountainous areas. *Mon. Wea. Rev.*, **121,** 1195–1214.

Brenner, S., 1993: Response of a large scale model to changes in eastern Mediterranean Sea surface temperature. *Isr. J. Earth. Sci.*, **39,** 125–130.

Haltiner, G. J., and R. T. Wiliams, 1980: *Numerical Prediction and Dynamic Meteorology.* John Wiley and Sons, Inc., 477 pp.

Israel Meteorological Service, 1985: *Bulletin of Rainfall in Israel 1984/85* (in Hebrew). Israel Meteorological Service, 32 pp.

Liu, W. T., K. B. Katsaros, and J. A. Businger, 1979: Bulk parameterization of air–sea exchanges of heat and water vapor including the molecular constraints at the interface. *J. Atmos. Sci.*, **36,** 1722–1735.

Rhea, J. O., 1978: Orographic precipitation model for hydrometeorological use. Ph.D. thesis, Colorado State University, 198 pp.

Rosenan, N., and M. Gilead, 1985: Rainfall, humidity, evaporation, climatic regions. *Atlas of Israel,* The Survey of Israel, 12 pp.

Shay-El, Y., and P. Alpert, 1991: A diagnostic study of winter diabatic heating in the Mediterranean in relation to cyclone. *Quart. J. Roy. Meteor. Soc.*, **117,** 715–747.

Tzvetkov, E., and G. Assaf, 1982: The Mediterranean heat storage and Israel precipitation. *Water Resour. Res.*, **18,** 1036–1040.

Wolfson, N., 1975: Topographical effects on standard normals of rainfall over Israel. *Weather,* **30,** 138–144.

Zangvil, A., and P. Druian, 1990: Upper air trough axis orientation and the spatial distribution of rainfall over Israel. *Int. J. Climatol.*, **10,** 57–62.